Fluid Dynamics and Co-located Conferences
24-27 June, 2013, San Diego, CA
31st AIAA Applied Aerodynamics Conference

AIAA 2013-3193

Propeller Induced Flow Effects on Wings at Low Reynolds Numbers

Gavin K. Ananda,* Robert W. Deters,† and Michael S. Selig‡
Department of Aerospace Engineering, University of Illinois at Urbana–Champaign, Urbana, IL 61801, USA

Significant performance benefits have been found for a wing with a propeller in the tractor configuration at low Reynolds numbers (30,000 to 80,000) based on the wing chord. Propeller induced flow experiments on a wing with an aspect ratio of 4 using the Wortmann FX 63-137 airfoil show that an increase in propeller rotation rate (decreasing advance ratio) results in lift-to-drag ratios as high as 10 to 12 (a maximum of 80% increase in lift-to-drag ratio from a clean wing configuration) at both low and high angles of attack up to stall (0 to 16 deg). Experiments performed using trips and upper surface oil flow visualization results show that the turbulated nature of the propeller slipstream induces early transition to turbulent flow over the central portion of the wing. The result is a reduction of pressure drag and an increase in lift of the wing. The effect is greatest at low angles of attack. Additionally, results are presented where the location of the propeller was varied with respect to the wing, including having the propeller in a pusher configuration. The results show that to maximize the performance of small-scaled unmanned aerial vehicles (UAV) it is critical to properly integrate the propeller in a way that minimizes adverse low Reynolds number flow effects on the aerodynamics of a small-scaled UAV.

Nomenclature

$\mathcal{AR}$	=	aspect ratio
b	=	wingspan
c	=	rectangular wing aerodynamic chord
C_L	=	wing lift coefficient ($= L/\frac{1}{2}\rho V_\infty^2 S_{ref}$)
C_D	=	wing drag coefficient ($= D/\frac{1}{2}\rho V_\infty^2 S_{ref}$)
$C_{M_{c/4}}$	=	wing moment coefficient at quarter chord ($= M/\frac{1}{2}\rho V_\infty^2 S_{ref} c$)
C_P	=	propeller power coefficient
C_T	=	propeller thrust coefficient
D	=	propeller diameter, drag
J	=	propeller advance ratio
L	=	lift
M	=	moment
n	=	propeller rotational rate in rotations per second
Q	=	propeller torque
Re	=	Reynolds number based on mean aerodynamic chord ($= V_\infty c/\nu$)
S_{ref}	=	wing reference area
V_∞	=	freestream velocity
α	=	wing angle of attack
η	=	propeller efficiency

*Graduate Student (Ph.D.), 104 S. Wright St., AIAA Student Member. anandak1@illinois.edu
†Graduate Student (Ph.D.), 104 S. Wright St., AIAA Student Member. rdeters@illinois.edu
‡Associate Professor, 104 S. Wright St., AIAA Senior Member. m-selig@illinois.edu

λ = taper ratio
ν = kinematic viscosity
ρ = density of air
Ω = propeller rotational rate

Subscripts

$c/4$ = quarter-chord

I. Introduction

The flow induced by a propeller refers to either the inflow or outflow (slipstream) of a propeller. The effect of propeller induced flow on the aerodynamic performance of a wing has been a subject of detailed research since the 1940s and 50s.[1–7] More recently, research has been conducted into the proper integration of the propeller-wing combination. In 1984, Loth and Loth[8] proposed that wing induced drag could be reduced through the use of wing-tip mounted propellers. The induced drag mitigating effects of wing-tip mounted propellers was confirmed experimentally and modelled numerically by Patterson and Bartlett,[9] and Miranda and Brennan[10] respectively.

Propeller-wing integration was taken a step further by Kroo,[11] who proposed that the wings designed for tractor configuration aircraft should be optimized based on the power-on propeller setting and not a clean wing. From Munk's stagger theorem,[12] Kroo showed that to minimize induced drag, wing airfoil section geometry, chord, and twist distribution should be modified for optimal lift distribution in the propeller-on configurations. Veldhius[13,14] advanced similar assertions to Kroo when he performed detailed experimental and numerical investigations into tractor configuration propeller-wing tests at a Reynolds number of approximately 400,000. In addition, from propeller positioning parametric studies, Veldhius found that higher vertical positions and negative propeller inclination angles with respect to the wing provided beneficial results.

Important steady-state propeller-wing interaction studies were also performed by Witkowski et al.[15,16] and Catalano.[17] Witkowski et al. showed aerodynamic performance improvements for wings under tractor configuration slipstream conditions. Tests performed on a semi-span wing at a Reynolds number of 470,000 showed typical lift curve slope increases of approximately 5.6% and drag reductions of approximately 65% at maximum propeller power. In addition, the effect of the wing on the aerodynamic characteristics of the propeller was found to be minimal. Catalano performed experiments on the effects of propeller induced flow on the aerodynamics of a Wortmann FX 63-137 wing at a Reynolds number of 350,000. Both pusher and tractor configurations were tested at varying positions and inclination angles. Results showed that whereas for tractor configuration cases, within the region of the slipstream, transition occurs close to the leading edge of the wing, for the pusher configuration, transition to turbulent flow is delayed.

The research discussed heretofore deals primarily with high Reynolds number flow. However, currently operational small-scaled UAVs tend to operate in the flight regime (Re = 30,000–300,000) that is primarily hampered by the adverse low Reynolds number effects of the laminar-separation bubble. Vehicles operating in this regime tend to be relatively inefficient (low lift-to-drag ratios) and difficult to predict.[18] In addition, most operational small-scaled UAVs are of low-to-moderate aspect ratios ($2 \leq \mathcal{R} \leq 7$) and therefore tend to have a significant portion of their wing located in the propeller induced flow region. The possible interactions between the three-dimensional wing effects, low Reynolds number effects, and the induced flow effects of the propeller in a small-scale UAV make it necessary to warrant further attention into the potential for performance improvements when performing propeller-wing integration.

At low Reynolds numbers, the effects of the induced flow of a propeller have been researched experimentally on low aspect ratio ($\mathcal{R} \leq 2$) Micro Air Vehicles (MAVs). The Micro Air Vehicle group at the University of Arizona has performed experimental testing of single and contra-rotating tractor-mounted propellers on low-aspect ratio wings at Reynolds numbers between 50,000 to 100,000.[19–22] Experimental results showed separation delay due to propeller slipstream flow and that at higher angles of attack, higher lift-to-drag ratio values were observed in comparison with wing only results. Flow visualization studies performed by

Sudhakar et al.[23] also confirm the separation delay effects discussed prior. Other than that, Gamble and Reeder[24] tested a MAV with an aspect ratio of 6.16. The effects of tractor configuration propeller-induced flow at various locations with respect to the wing were presented at an angle of attack of zero degrees.

The limited amount of literature at low Reynolds numbers suggests that there is a need to expand the understanding of propeller-induced flow effects on wings at low Reynolds number. To accomplish this goal, experiments were conducted where a Wortmann FX 63-137 rectangular wing with an aspect ratio of 4 was tested with a GWS 5×4.3 micro propeller at Reynolds numbers between 50,000 and 80,000. Various parameters were varied during testing. These include propeller advance ratio, propeller location, and chordwise Reynolds number. In addition to presenting wind tunnel results, oil flow visualization results are presented and discussed.

II. Experimental Methods

A. Facility

The facility used for all experiments was the low turbulence subsonic wind tunnel located at the Aerodynamic Research Lab at the University of Illinois at Urbana-Champaign (UIUC). The wind tunnel is an open-return tunnel with a rectangular test section that measures 2.8×4.0 ft (0.853×1.219 m) in cross-section and 8 ft (2.438 m) in length. Over the length of the test section, the width of the tunnel cross section increases by approximately 0.5 in (12.7 mm) to account for boundary layer growth along the tunnel side walls. Test section speeds up to 160 mph (71.53 m/s) can be obtained via a 125 hp (93.25 kW) alternating current electric motor connected to a five-bladed fan. As detailed in Ref. 25, the turbulence intensity of the wind tunnel was measured to be less than 0.1%.

B. Experimental Setup

The experimental setup consisted of two main independent components: a three-component platform force balance (LRN-FB) and the propeller fairing setup as depicted in Fig. 1. The LRN-FB measured the aerodynamic loads of the wing under different propeller induced flow conditions. The propeller fairing setup provided the wing with the specific propeller induced flow conditions.

The LRN-FB was a custom designed and in-house fabricated external three-component platform force balance. The design, assembly, and validation of the LRN-FB are described in detail in Refs. 26 and 27.

The propeller fairing setup was designed to generate the induced flow of a propeller thereby allowing for its effects on the aerodynamics of the wing to be directly measured. The propeller fairing setup could be placed in either a tractor or pusher configuration. Shown in Fig. 2, the propeller fairing setup consisted of five main components, the horizontally-mounted fairing structure, the motor-propeller combination, the vertically-placed connecting rods, the square-flange mounts, and the mouting plates.

The horizontally-mounted fairing structure was rapid prototyped using stereolithography (SLA®). The fairing structure housed a Medusa 12-mm (0.47-in) diameter 4000 kV Afterburner inrunner motor. The motor had a 1.5-mm (0.059-in) shaft and the ability to test 2–5-in (50.8–127-mm) diameter propellers without the need of a gearbox. The wires that powered the motor ran through the SLA fairing structure to a Castle Creations Pheonix-10 speed controller. The speed controller (and motor) was powered by a variable power supply.

The fairing structure was mounted horizontally in the tunnel test section using two connecting rods that had 0.5"-20 threaded male ends. The connecting rods were mounted on mounting plates via square-flange mounts. The square-flange mounts maintained the rigidity of the connecting rods and fairing structure during tests. The multiple holes located on the mounting plates gave the propeller fairing setup the ability to change its location with respect to the wing. Furthermore, the mounting plates were attached to the UIUC main platform balance, whose center of rotation was aligned with that of the LRN-FB and the wing quarter-chord. The center of rotation alignment gave the propeller fairing the ability to match its angle of attack with that of the wing during angle-of-attack sweep runs. In addition, an incidence angle could also be set for the propeller fairing setup with respect to the wing angle of attack.

C. Data Acquisition

A PC with a National Instruments NI PCI-6052E data acquisition board was used for communication with the wind tunnel, LRN-FB, and propeller fairing setup. Test section dynamic pressure was measured with a differential pressure transducer in the wind tunnel inlet and test section. Ambient temperature was measured with a thermocouple. Lift, drag, and moment data from the load cells in the LRN-FB were passed through a signal conditioner to amplify and filter the signals for the DAQ board. At each angle of attack, 30,000 contiguous samples of lift, drag, and moment were measured at a rate of 3,000 samples/s and averaged to overcome the small time-dependent fluctuations in the measurements. Each run involved taking measurements of the wing for both increasing and decreasing angles of attack in succession to capture any possible aerodynamic hysteresis. The DC angle-of-attack motor was controlled via a custom-designed motor controller and supporting driver software.

For the propeller fairing setup, control of the Medusa inrunner motor was done through the PC via a servo exciter connected to the speed controller. A red laser with a wavelength of 630–680 nm and a phototransistor with a rise time of 5 μs was used to measure the RPM of the propeller. The laser was placed outside the test section and directed to ensure that the propeller, when spinning, blocked the laser from the photo-transistor that was located on the opposing side of the test section. As the propeller spins, the propeller blades block the laser beam, and the receiver output voltage drops to zero from a voltage of at least 2 V. The voltage was measured by the DAQ board at a rate of 40,000 samples/s for 30,000 samples. The high rate and sample number ensured that the resulting square waves were captured and voltage peaks counted. The RPM is then counted by dividing the number of peaks by the sample time and the number of propeller blades. During runs, the LabVIEW code adjusted the voltage sent to the servo exciter to achieve a pre-specified propeller RPM.

During a run, the entire data-acquisition process was automated. The National Instruments LabVIEW® graphical user interface set and maintained the Reynolds number of the wind tunnel, the RPM of the motor, the angle of attack of the wing, the angle of attack of the propeller and acquired raw data. The raw data was

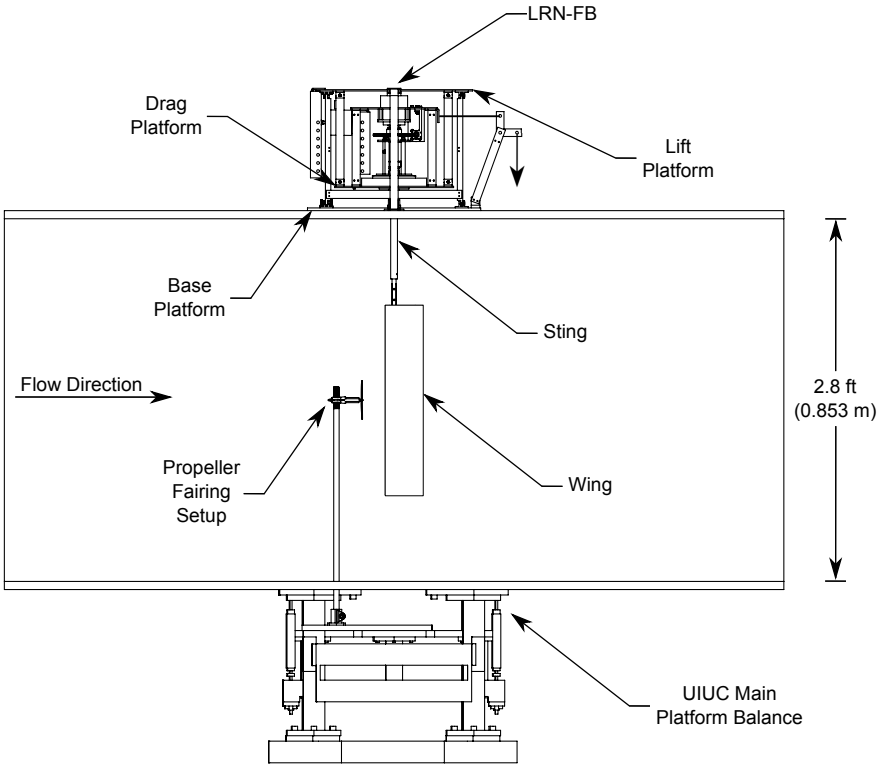

Figure 1. UIUC LRN-FB and propeller fairing setup in the tunnel test section (tractor configuration).

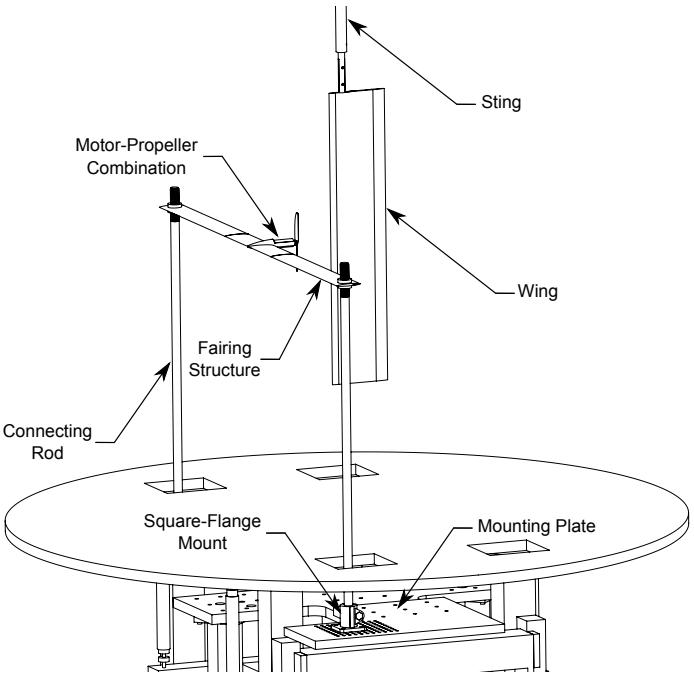

Figure 2. Isometric view of the propeller fairing setup in tunnel test section (tractor configuration).

then reduced and plotted graphically during a run for realtime inspection. Once the run was complete, the data was corrected for three-dimensional tunnel effects according to the methods outlined in Ref. 28. Note that the corrections performed did not account for the propeller fairing setup. The relative uncertainties of the lift, drag, and moment coefficients were calculated to be 3.3%, 2.7%, and 4.6%, respectively, using the methods introduced by Kline and McClintock[29] and further discussed by Coleman and Steel.[30]

D. Models Tested

All experiments were performed using a rectangular (λ=1) wing with a Wortmann FX 63-137 airfoil and a 5×4.3 micro propeller manufactured by GWS. The Wortmann wing had an aspect ratio ($\mathcal{AR}$) of 4 and was rapid prototyped using SLA® to tolerances of approximately ±0.005 in,[31] ensuring model accuracy and surface quality. The wing had a chord length (c) of 3.5 in (88.9 mm). Performance data for the Wortmann FX 63-137 wing at low Reynolds numbers (30,000 to 100,000) can be found in Refs. 26 and 27.

The GWS 5×4.3 micro propeller had a diameter of 5 in and a pitch of 4.3 in. It was chosen as there was performance data available, and the diameter was appropriate given the 3.5 in chord length of the Wortmann wing. The performance data for the GWS 5×4.3 micro propeller are presented and discussed in Section III.

E. Propeller Induced Flow Conditions

Three main propeller induced flow effects are presented in this paper: the effect of varying the propeller advance ratio (J) and its location parallel (X) and perpendicular (Z) to the wing. The propeller advance ratio (J) was varied by changing the rotation rate of the propeller. The location of the propeller was varied in the longitudinal plane located at the midspan of the wing. Measurements were taken with the origin located on the wing rotation axis (LRN-FB centerline) as shown in Fig. 3.

The X axis of the measurement system is defined as being parallel to the chordline of the wing with the origin at the rotation axis of the wing. Given that the Wortmann wing was cambered, the X axis is located 0.17 in (4.44 mm) above the chordline of the wing as shown in Fig. 4. The Z axis of the measurement system is perpendicular to the X axis of the wing. Propeller location measurements are taken from the center of

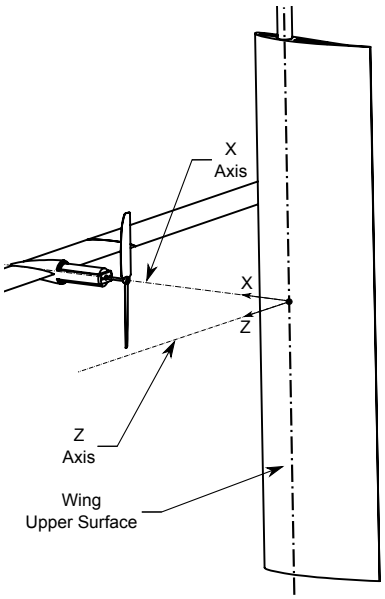

Figure 3. Measurement axis system for locating the propeller with respect to the wing.

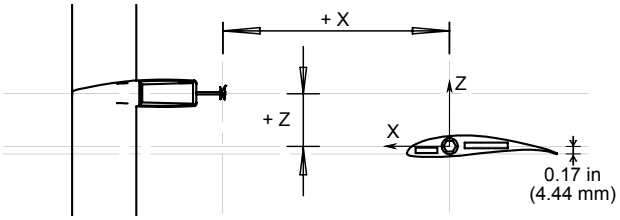

Figure 4. Longitudinal plane of the wing showing the origin of the measurement system with the propeller fairing setup in a tractor configuration.

the hub of the propeller and are normalized by the diameter of the propeller. To aid in the presentation of results later in the paper, the six different propeller locations tested are tabulated in Table 1.

Table 1. Propeller Positions Tested

Position Number	X Location	Z Location
1	0.725 D	0 D
2	0.475 D	0 D
3	0.265 D	0 D
4	−0.705 D	0 D
5	0.725 D	0.25 D
6	0.725 D	−0.25 D

III. GWS 5×4.3 Propeller Performance

Performance data for the GWS 5×4.3 micro propeller was gathered using a wind tunnel testing rig designed to measure propeller thrust and power. More information on the setup and procedure to test these propellers can be found in Deters et al.[32] and Brandt.[33] An Interface SMT S-Type load cell with a load capacity of 2.2 lb (9.8 N) measured thrust, and a Transducer Techniques RTS-5 5 oz-in (0.0353 N-m) torque cell was used to measure torque. From the torque measurements, the power was calculated by

$$P = 2\pi n Q \tag{1}$$

where n is the rotational speed measured in rotations per second and Q is the torque. Thrust and power coefficients (C_T and C_P) were calculated using the rotational speed and diameter respectively with the following equations

$$C_T = \frac{T}{\rho n^2 D^4} \tag{2}$$

$$C_P = \frac{P}{\rho n^3 D^5} \tag{3}$$

For static conditions, the propellers were tested over a range of rotational speeds, and for tests with a freestream velocity, the propellers were tested over a range of advance ratios (J) calculated by

$$J = \frac{V}{nD} \tag{4}$$

During freestream velocity tests (wind tunnel on), the propeller was set to run at a constant rotational speed, and the flow speed was increased from 4 ft/s to a flow speed near the onset of windmilling. The efficiency of the propeller during these tests was also calculated by

$$\eta = \frac{C_T J}{C_P} \tag{5}$$

Results from the performance tests for the GWS 5×4.3 propeller are shown in Figs. 5 and 6. The static thrust and power coefficients are shown in Fig. 5, and the thrust coefficient, power coefficient, and efficiency with a freestream velocity are shown in Figs. 6(a)–6(c). Note that the Reynolds number displayed in Figs. 5 and 6 is for the propeller and is defined by the chord and rotational speed at the 75% blade station.

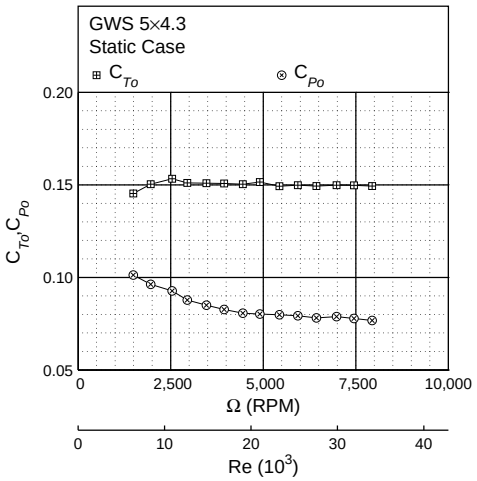

Figure 5. GWS 5×4.3 static performance data.

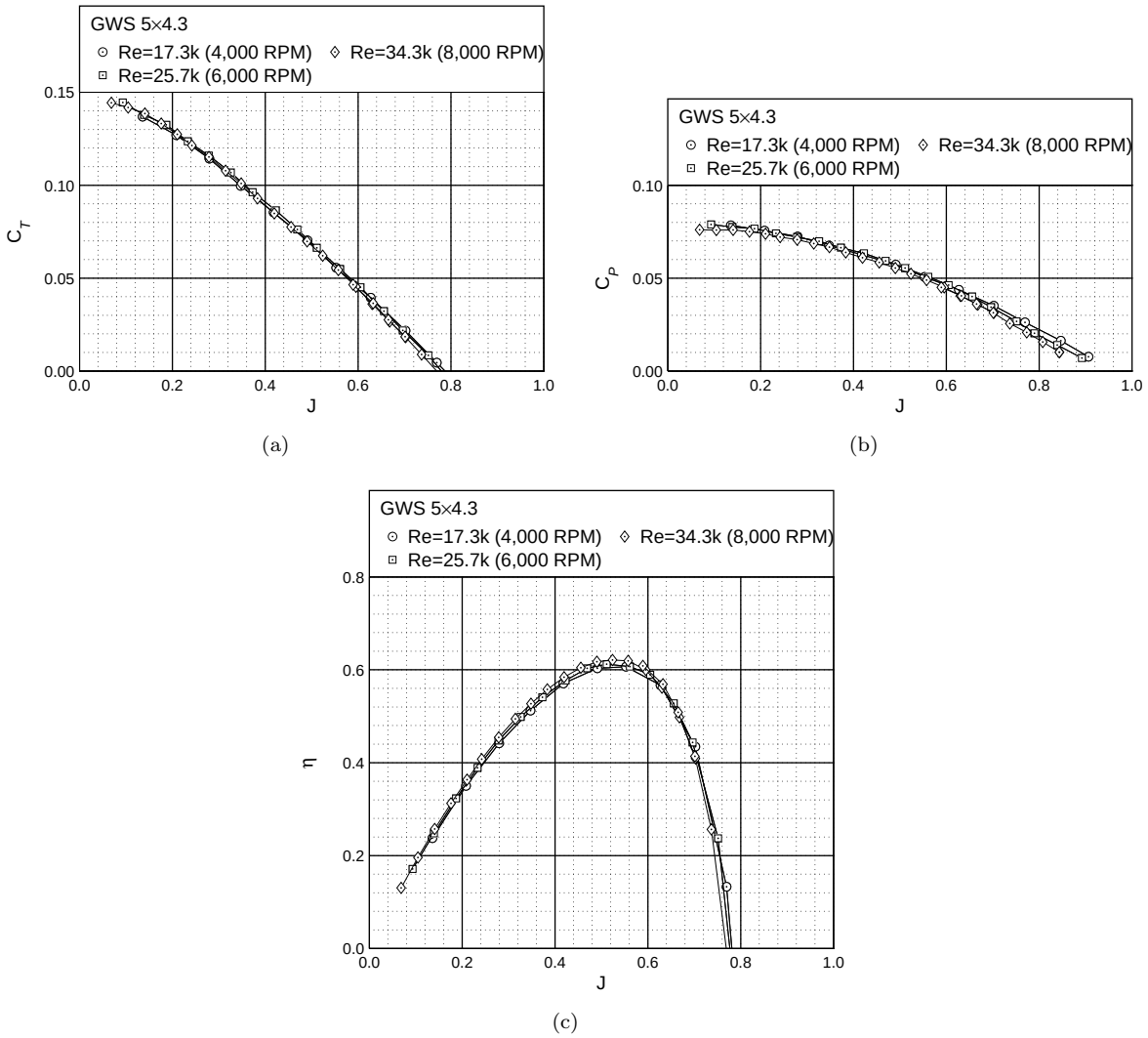

Figure 6. GWS 5×4.3 performance data: (a) thrust coefficient, (b) power coefficient, and (c) efficiency curve.

IV. Effect of Propeller Fairing Setup

Prior to presenting the effects of propeller induced flow on the aerodynamic performance of wings, the effects of the propeller fairing setup alone (no propeller) on the aerodynamics of the wing are presented. A comparison was performed on the Wortmann wing results for a clean configuration case, tractor configuration propeller fairing case (Position 1), and a pusher configuration propeller fairing case (Position 4). A full set of results for the clean configuration case at low Reynolds number (30,000 to 100,000) can be found in Ref. 27. Drag polars are presented in Figs. 7(a–d) for the Reynolds numbers of 60,000 to 90,000 to chart the difference between the three configurations.

The results in Figs. 7(a–d) show that the propeller fairing setup in a tractor configuration influences the aerodynamic properties of the wing at Reynolds numbers close to when the separation bubble forms on the Wortmann FX 63-137 wing. The effect of the tractor configuration propeller fairing setup is such that the separated flow from the setup induces the formation of a separation bubble on the Wortmann wing at lower Reynolds numbers than that of the clean or pusher configuration. In the pusher configuration, the propeller fairing setup is located behind the wing so it does not affect the turbulence of the flow that the Wortmann wing encounters. Therefore minimal differences are observed between the pusher and clean configuration results. The effect of the tractor configuration propeller fairing setup on the flow over the upper surface of

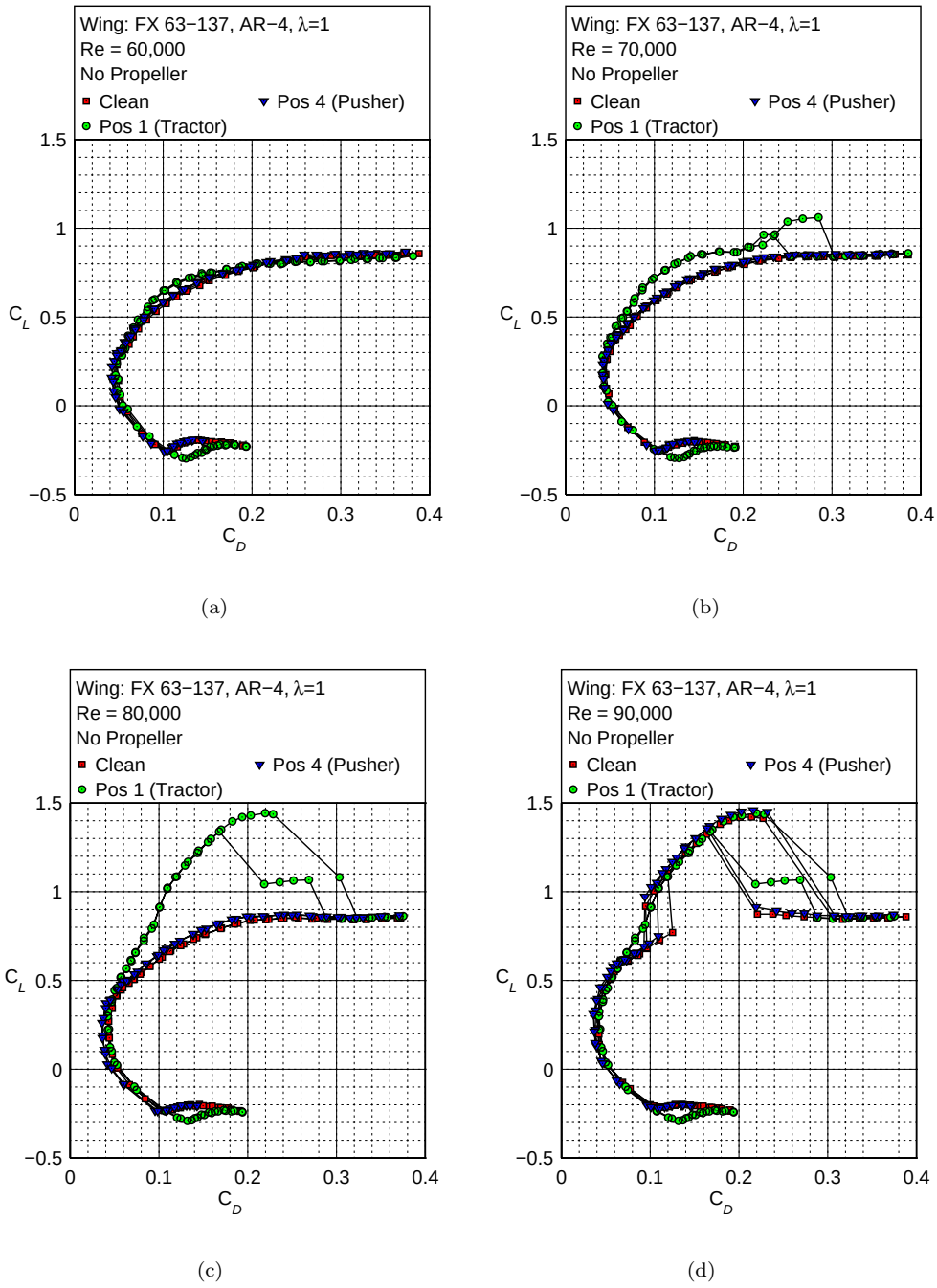

Figure 7. Wortmann FX 63-137 *AR*-4 rectangular wing drag polars with different propeller fairing setup configurations: (b) Re = 70,000, (c) Re = 80,000, (c) Re = 80,000, and (d) Re = 90,000.

the Wortmann wing can also be observed from surface oil flow visualization tests performed as shown in Figs. 8(a,b). A region of turbulent flow roughly the width of the motor mount of the propeller fairing setup and a separation bubble over the rest of the wing is created at a Reynolds number of 80,000 due to the separated flow from the propeller fairing setup.

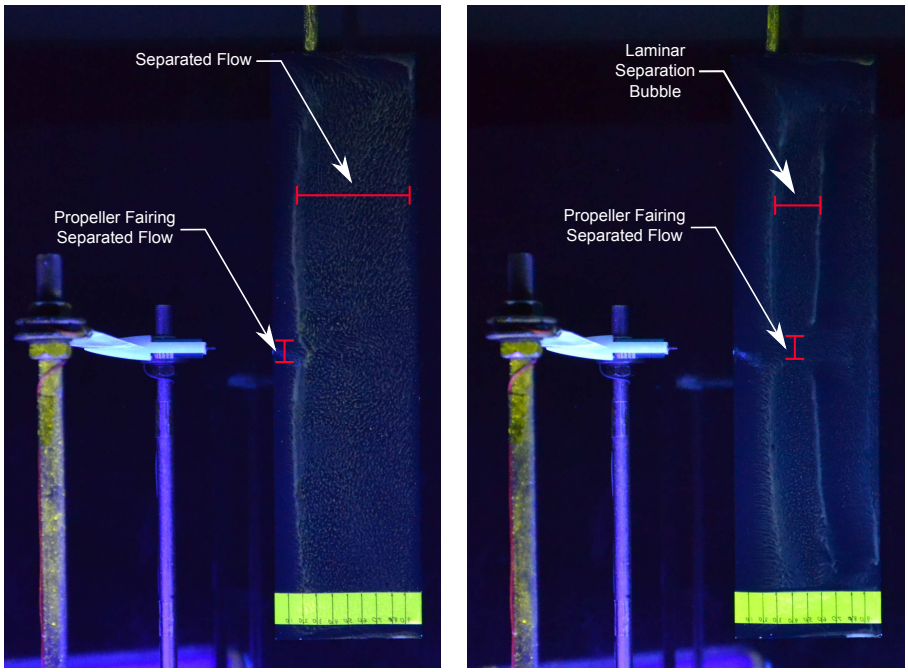

(a) (b)

Figure 8. Upper surface oil flow visualization results of the Wortmann FX 63-137 AR-4 rectangular wing with tractor configuration propeller fairing setup (no propeller) at an angle of attack of 9 deg: (a) Re = 60,000 and (b) Re = 80,000.

V. Propeller Induced Flow Experiments

All propeller induced flow experiments were conducted between the wing chordwise Reynolds numbers of 50,000 to 80,000. A maximum Reynolds number of 80,000 was chosen as that was the Reynolds number at which the GWS 5×4.3 propeller was in a brake state (negative C_T) at the maximum propeller rotation rate (Ω) tested of 7,000 RPM.

A. Effect of Propeller Advance Ratio

The effect of varying the GWS 5×4.3 propeller advance ratio on the performance of the Wortmann wing was tested at propeller rotation rates, Ω, of 5,000 RPM and 7,000 RPM at Position 1 corresponding to the tractor configuration. The propeller advance ratio, J, is calculated using Eq. 4. Lift, drag, lift-to-drag ratio, and moment curves as a function of angle of attack are presented in Figs. 9–11 to show the propeller advance ratio effects at wing chord Reynolds numbers of 60,000 and 80,000.

The lift curves in Figs. 9(a) show large increases in $C_{L_{max}}$ due to decreasing propeller advance ratio for the Reynolds number of 60,000 case. An increase in $C_{L_{max}}$ is not observed for the Reynolds number of 80,000 case as the propeller is in a brake state (negative C_T). A propeller in this state causes a decrease in flow speed in the propeller slipstream region compared with the rest of the wing. Therefore, a slight decrease in $C_{L_{max}}$ is observed. Both figures also show an increase in the stall angle of attack with decreasing advance ratio. In addition, the zero-lift angle of attack decreases with advance ratio. The 'effective camber' effect discussed by Witkowski and Sullivan[16] and an increase in lift curve slope mentioned in Refs. 15, 16, and 17 is observed for the Reynolds number of 60,000 case.

Drag results from Figs. 10(a,b) show a pronounced reduction in drag at low and higher angles of attack (−2 to 15 deg). The results observed suggest that apart from the reduction in induced drag discussed in literature, there also appears to be a reduction in the pressure (form) drag of the wing. The reduction in drag cannot solely be attributed to the increase in flowspeed (for the Re = 60,000 case) over a portion of the wing

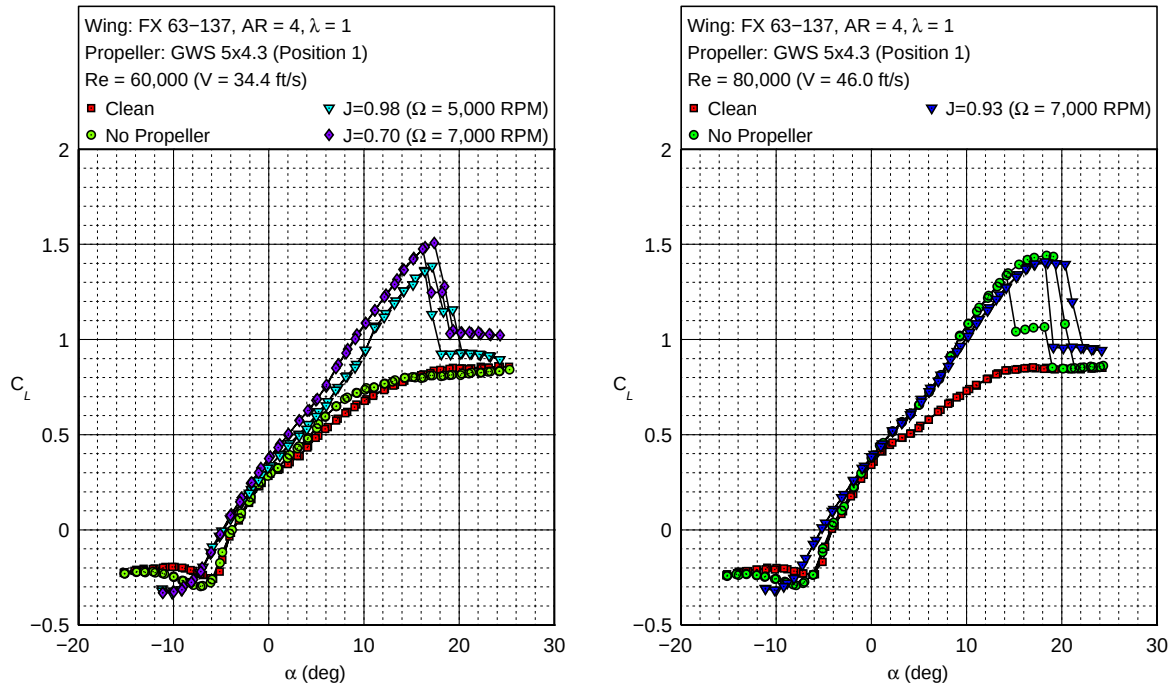

(a) (b)

Figure 9. Effect of increasing propeller advance ratio on the lift curve of the Wortmann FX 63-137 *AR*-4 rectangular wing at Reynolds numbers of (a) 60,000 and (b) 80,000.

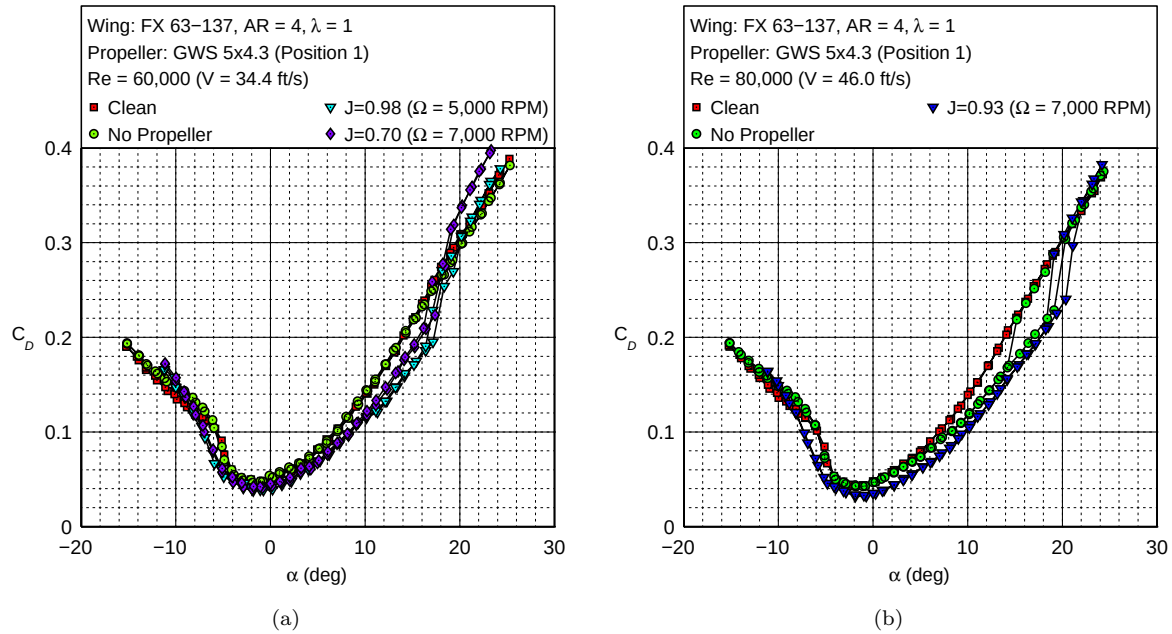

(a) (b)

Figure 10. Effect of increasing propeller advance ratio on the drag curve of the Wortmann FX 63-137 *AR*-4 rectangular wing at Reynolds numbers of (a) 60,000 and (b) 80,000.

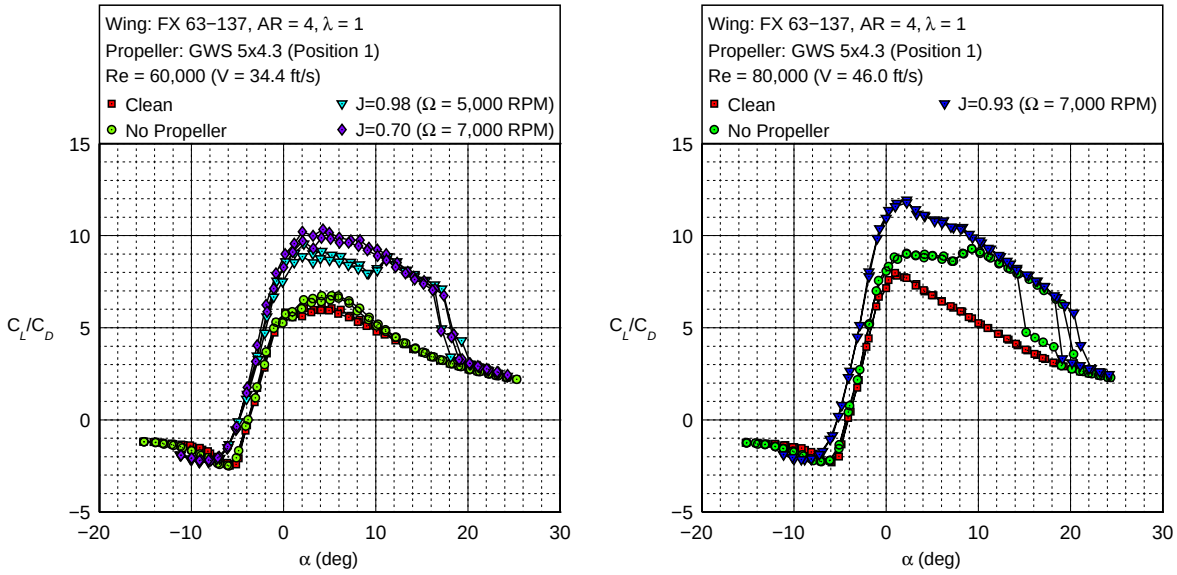

Figure 11. Effect of increasing propeller advance ratio on the lift-to-drag ratio curve of the Wortmann FX 63-137 *AR*-4 rectangular wing at Reynolds numbers of (a) 60,000 and (b) 80,000.

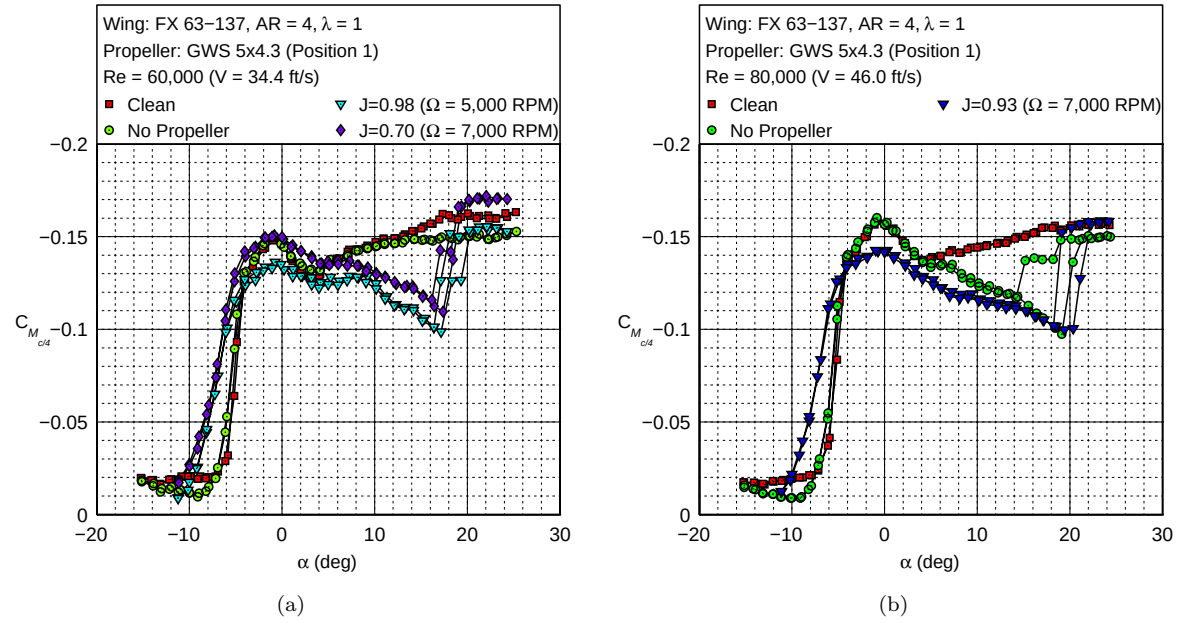

Figure 12. Effect of increasing propeller advance ratio on the moment curve of the Wortmann FX 63-137 *AR*-4 rectangular wing at Reynolds numbers of (a) 60,000 and (b) 80,000.

as the reduction in drag observed in the Reynolds number of 80,000 case occurs when the propeller was in a brake state, meaning that the induced flow due to the propeller seems to act like a trip in turbulating the flow over the wing. These observations are further reinforced by the C_L/C_D curves presented in Figs. 11(a,b). The results show that a significant increase in the lift-to-drag ratio (a maximum of 80% increase is observed from the clean configuration) at most angles of attack before stall for both Reynolds number cases. Although

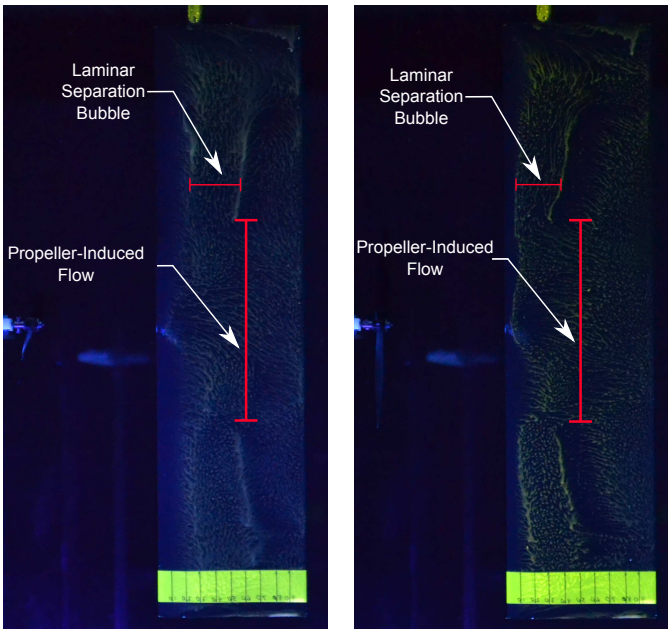

(a) (b)

Figure 13. Upper surface oil flow visualization results of the Wortmann FX 63-137 AR 4 rectangular wing with a tractor configuration GWS 5×4.3 propeller running at a propeller rotation rate of 7,000 RPM and chordwise Reynolds number of 60,000: (a) α=9 deg and (b) α=14 deg.

at a Reynolds number of 80,000 the propeller is in a brake state, the induced flow from the propeller still creates a large increase in the lift-to-drag ratio at low angles of attack due to a reduction in form drag (pressure drag from laminar separation or the laminar separation bubble) caused by the turbulated propeller slipstream region over the wing. From Figs. 12(a,b), the moments observed closely match those found at higher Reynolds numbers for the clean configuration.

The effects of propeller advance ratio on a Wortmann wing with otherwise fully separated flow is shown with upper surface oil flow visualization results in Figs. 13(a,b). The formation and movement of the laminar separation bubble towards the leading edge with angle of attack is shown. Also, a region of turbulated flow roughly the size of the propeller is seen on the upper surface of both figures due to the induced flow from the propeller. The propeller induced flow creates this turbulated region at most angles of attack and also induces the reattachment of the flow over the rest of the wing.

To further understand the effect of the induced flow of the propeller in turbulating the flow over the Wortmann wing, experiments were performed where trips that were the span of the propeller (5 in) were placed on the upper surface of the Wortmann wing as shown in Figure 14. Based on surface oil flow visualization results, the trip tape was placed with its aft located at the 10% chord length to ensure that the trip turbulated the flow ahead of when laminar separation occurred. The trip tape dimensions were 0.125 in. (3.175 mm) in width and 0.0045 in. (0.1143 mm) in thickness. The change in lift-to-drag ratio ($\Delta C_L/C_D$), lift (ΔC_L), and drag (ΔC_D) of the Wortmann wing from the clean configuration is presented for the Reynolds numbers of 60,000 and 80,000 in Figs. 15–17.

As discussed previously, the tractor configuration propeller fairing setup with no propeller affects the aerodynamics of the wing. The effect is minimal at a Reynolds number of 60,000 as for this case the laminar separation bubble has not formed [see Fig. 15(a)]. For the Reynolds number of 80,000 case [see Fig. 15(b)], however, reattachment is induced at higher angles of attack by the propeller fairing setup. The trips with no propeller case performs similarly in that reattachment of the laminar separated flow occurs at angles of attack starting at 2 deg for the Reynolds number of 80,000 case. In addition, for the Reynolds number of 60,000 case, the trips induce the formation of the separation bubble at angles of attack larger than 10 deg.

It can be also observed from Figs. 15(a,b) that the tractor propeller-on configuration augments the lift-

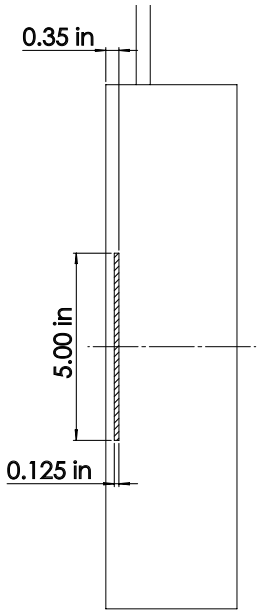

Figure 14. Wortmann FX 63-137 $\mathcal{AR}$-4 rectangular wing with 0.0045-in. thick trip tape aft edge located at 10% chord (0.35 in).

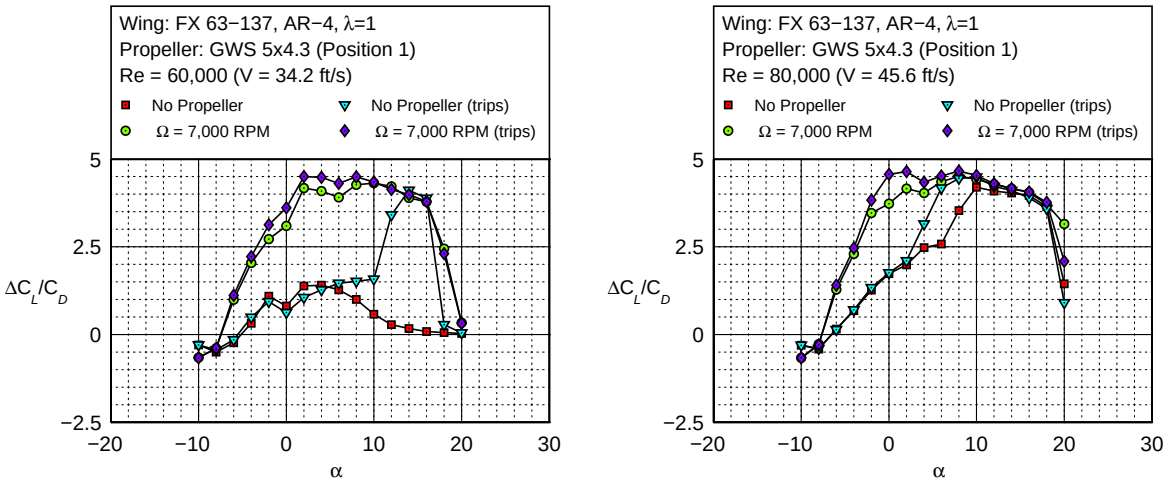

Figure 15. Effect of the GWS 5×4.3 propeller advance ratio and trips on the Wortmann FX 63-137 $\mathcal{AR}$-4 rectangular wing $\Delta C_L/C_D$ curve at different Reynolds numbers: (a) Re = 60,000 and (b) Re = 80,000.

to-drag ratio of the wing at all angles of attack. The augmentation of lift-to-drag ratio close to the zero-lift angle of attack (≈ -5 deg) occurs as a result of an increase in lift [see Figs. 16(a,b)] and a decrease in pressure drag [see Figs. 17(a,b)]. As the angle of attack increases for the Reynolds number of 60,000 case, lift-to-drag ratio augmentation occurs mainly due to the increase in lift and decrease in drag because of the reattachment of the separation bubble. Even for the brake-state case (Re = 80,000), the effect of the propeller induced flow in turbulating the flow that the wing encounters is clearly observed at low angles of attack (-5 to 5 deg) in Fig. 15(b) thereby augmenting the lift-to-drag ratio of the wing.

It can be concluded that the effect of increasing the propeller advance ratio in a tractor configuration is

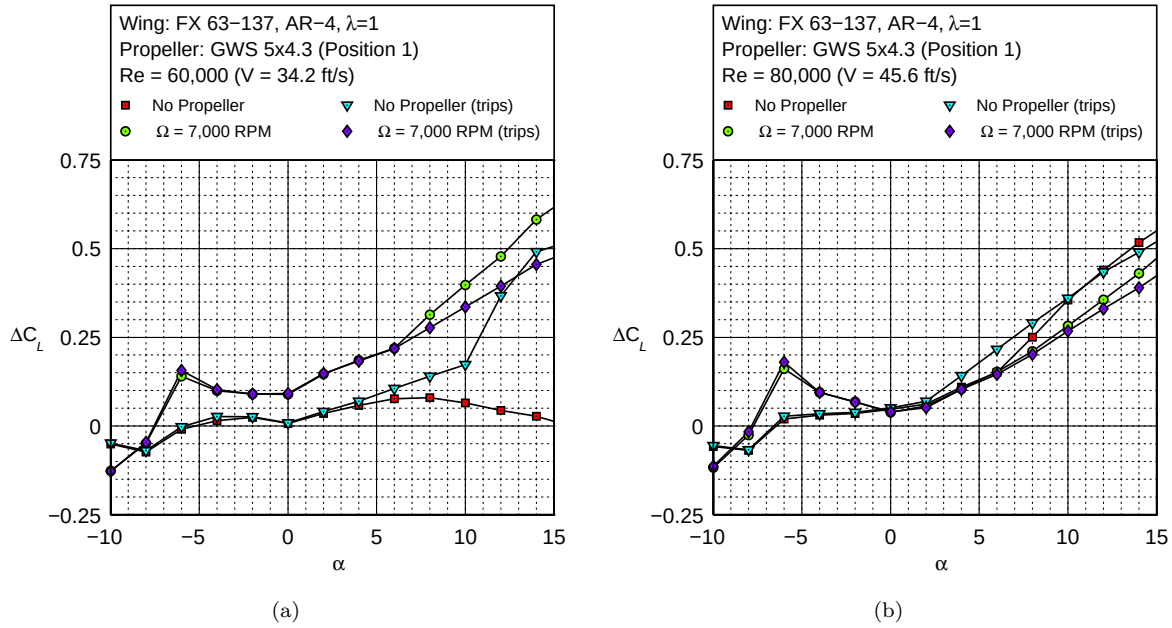

Figure 16. Effect of the GWS 5×4.3 propeller advance ratio and trips on the Wortmann FX 63-137 *AR*-4 rectangular wing ΔC_L curve at different Reynolds numbers: (a) Re = 60,000 and (b) Re = 80,000.

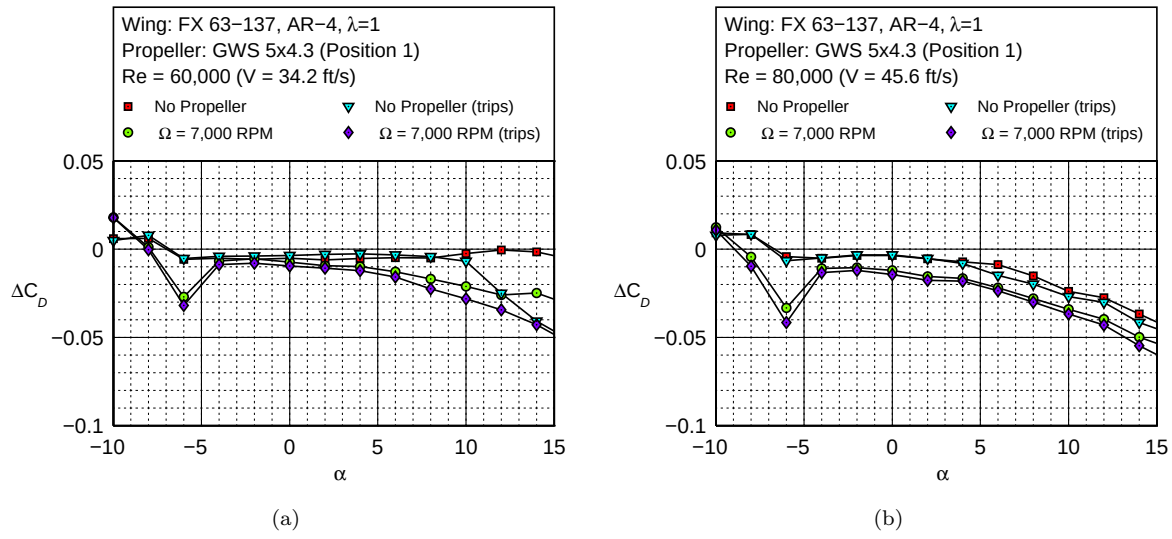

Figure 17. Effect of the GWS 5×4.3 propeller advance ratio and trips on the Wortmann FX 63-137 *AR*-4 rectangular wing ΔC_D curve at different Reynolds numbers: (a) Re = 60,000 and (b) Re = 80,000.

significant at low Reynolds numbers. The turbulated nature of the induced flow due to the propeller creates the centrally turbulated region over the wing and induces the formation of the separation bubble outside this region thereby contributing towards the significant augmentation of the lift-to-drag ratio, most importantly at low angles of attack.

B. Effect of Propeller X Location

All tests done previously had been with the GWS 5×4.3 propeller located at Position 1. The effect of varying the propeller X location was then tested by setting the propeller fairing setup at four separate locations: Positions 1, 2, 3 (tractor configurations), and 4 (pusher configuration). Performance results are presented for the Wortmann wing at a Reynolds number of 70,000 with the GWS propeller rotation rate at 7,000 RPM in Figs. 18(a,b) and 19(a–d).

Upon observation of Figs. 18(a,b), it is evident that the propeller in a pusher configuration (Position 4) exhibits different aerodynamic performance characteristics for the Wortmann wing in comparison with the propeller in a tractor configuration (Positions 1, 2, and 3). As Catalano[17] stated, the effect of the propeller induced flow in the pusher configuration is to delay separation and the move the laminar separation point further aft on the wing. The lift and lift-to-drag ratio curves for the propeller in pusher configuration are seen to exhibit laminar flow characteristics at angles of attack less than 10 deg. At an angle of attack of 10 deg, the separation bubble forms and a jump in lift and lift-to-drag ratio occurs. The delayed formation of the separation bubble is caused by the induced flow from the propeller in pusher configuration extending the laminar flow separation point further aft of the wing. The flow does not reattach at low angles of attack resulting in a minimal increase in lift and decrease in drag from the clean configuration. Therefore the augmentation of lift-to-drag ratio observed in the tractor configuration results for low angles of attack is not observed for the pusher configuration results [see Fig. 18(b)]. At higher angles of attack, however, the increased flow velocity over a portion of the wing induces the creation of the separation bubble thereby allowing for the lift-to-drag ratios to match those in the tractor configuration.

Given that the differences between the three tractor configurations are very close, results are presented in terms of the change (Δ) of the aerodynamic performance characteristics from the clean configuration as shown in Figs. 19(a–d). It can be observed between the three tractor configurations (Positions 1, 2, and 3) that there is an increase in C_L/C_D with decreasing X distance from the wing [see Fig. 19(d)] at angles of

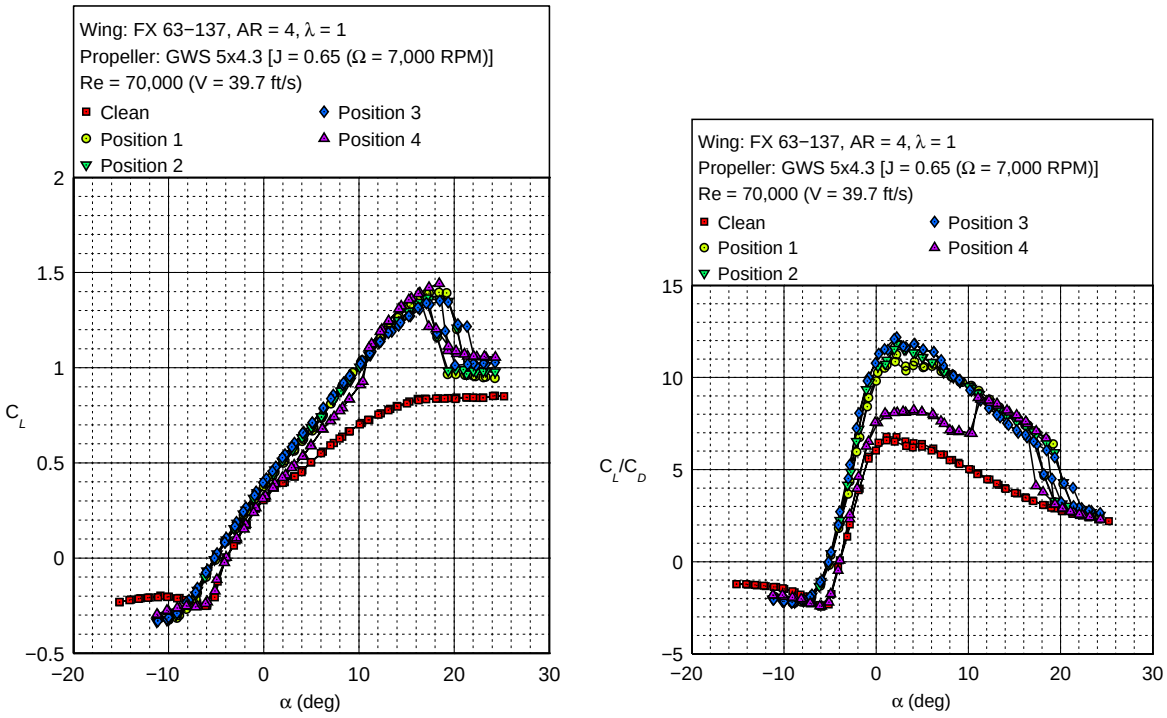

Figure 18. Effect of the GWS 5×4.3 propeller X location on the Wortmann FX 63-137 AR-4 rectangular wing at a Reynolds number of 70,000 and propeller rotation rate of 7,000 RPM: (a) lift curve and (b) lift-to-drag ratio curve.

attack lower than 9 deg. The increase in C_L/C_D is mostly due to an increase in the lift of the wing with decreasing propeller distance from the wing [see Fig. 19(a)]. At higher angles of attack ($\geq$ 10 deg) though, the effects are reversed with lower lift and lift-to-drag ratios observed.

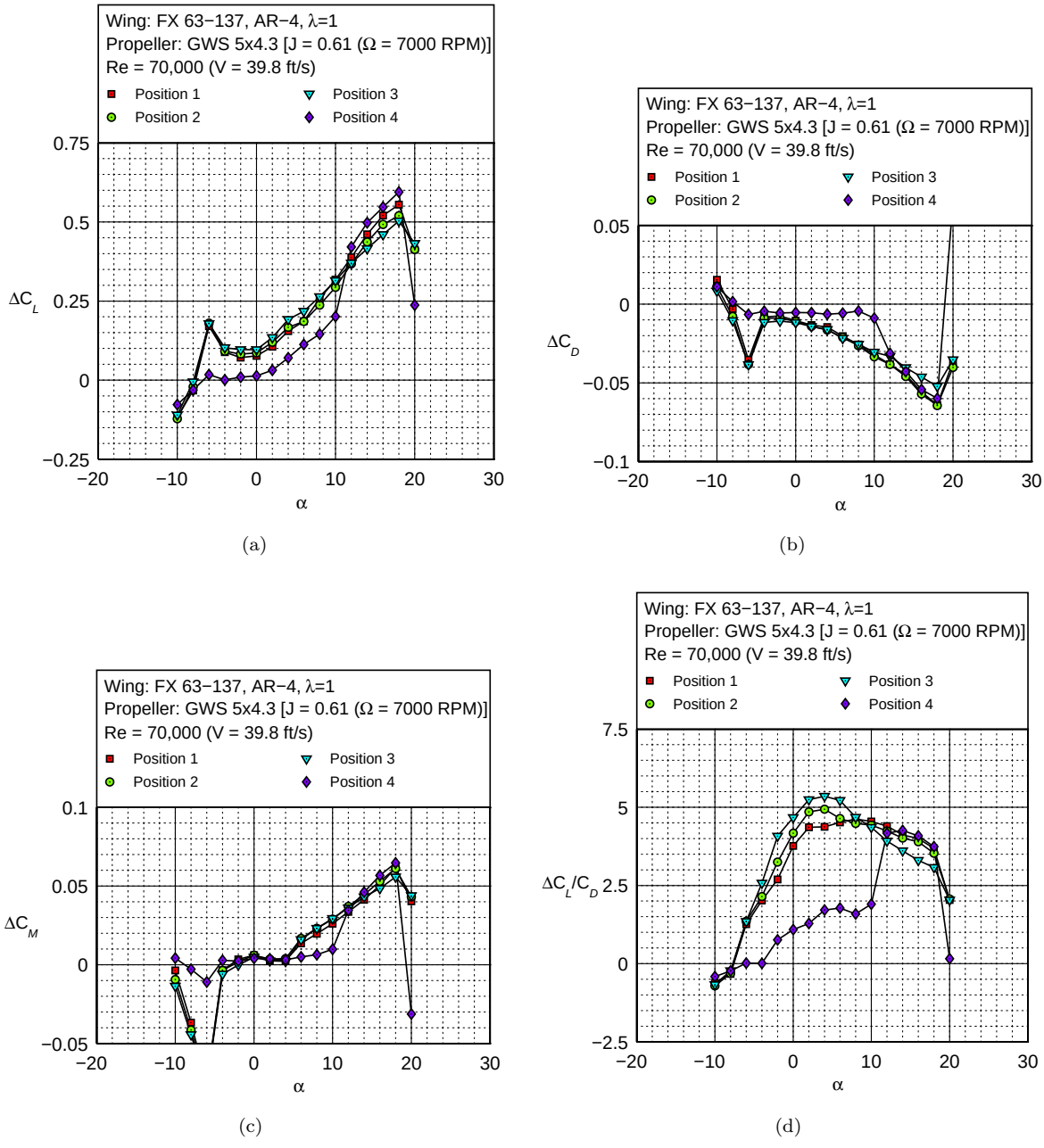

Figure 19. Effect of varying propeller X location with respect to the Wortmann FX 63-137 $\mathcal{AR}$-4 rectangular wing at a Reynolds number of 70,000 and propeller rotation rate of 7,000 RPM: (a) ΔC_L, (b) ΔC_D, (c) ΔC_M, and (d) $\Delta C_L/C_D$.

C. Effect of Propeller Z Location

The effect of varying the Z location of the GWS 5×4.3 propeller is shown by presenting aerodynamic performance results between the propeller in Positions 1, 5, and 6. Performance results are presented for the Wortmann wing at a Reynolds number of 70,000 with the GWS propeller rotation rate at 7,000 RPM

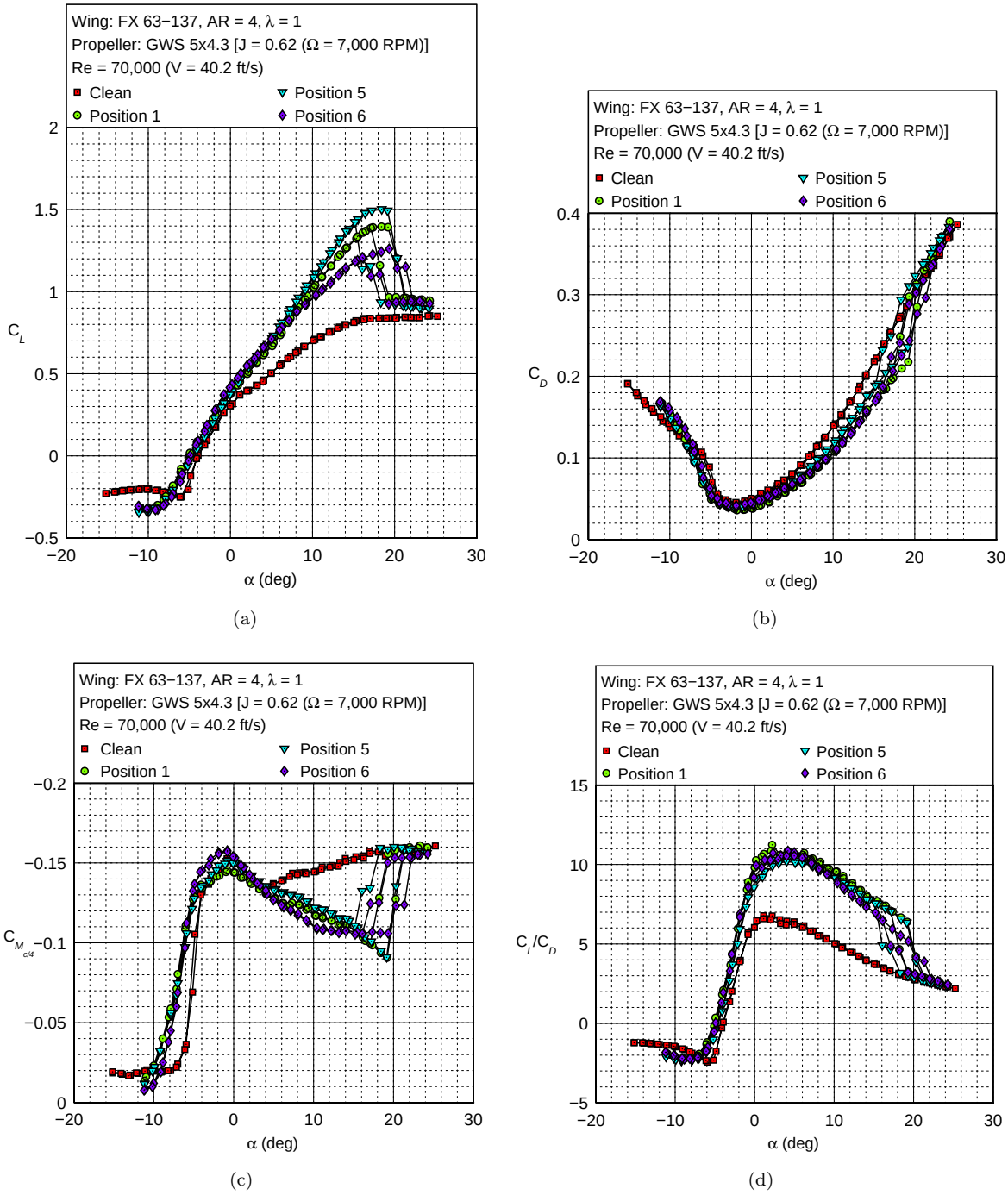

Figure 20. Effect of the GWS 5×4.3 propeller Z location on the Wortmann FX 63-137 AR-4 rectangular wing at a Reynolds number of 70,000 and propeller rotation rate of 7,000 RPM: (a) lift curve, (b) drag curve, (c) moment curve, and (d) lift-to-drag ratio curve.

in Figs. 20(a–d).

The effect of varying the propeller Z location is mainly observed at higher angles of attack ($\alpha \geq 10$ deg). The propeller with its axis located below the wing (Position 6) does not augment the lift of the wing as well as the propeller located above the wing (Position 5) [see Fig. 20(a)]. Although a lower drag change at high angles of attack was observed for the above wing propeller configuration, the end result is such that the propeller with its axis located below the wing results in a lower lift-to-drag ratio increase from the clean configuration [see Fig. 20(d)]. Minimal variation was observed in the moment of the wing at all angles of attack as shown in Fig. 20(c).

VI. Conclusions

A review of literature suggested that in the low Reynolds number (30,000 to 80,000), low-to-moderate aspect ratio wing ($2 \leq \mathcal{AR} \leq 5$) regime there was a lack of data that related to the effect of the induced flow of a propeller on the performance of a wing. A majority of small-scaled fixed wing UAVs operate with a significant portion of their wing located in the slipstream of the propeller. Therefore, an experimental setup was created that allowed for different parameters related to the propeller location and advance ratio (J) with respect to the wing to be tested easily.

The experiments presented in the paper were done using the Wortmann FX 63-137 rectangular wing with an aspect ratio of 4 and a GWS 5×4.3 propeller. Results were presented for the effects of varying the propeller advance ratio and propeller location. An important conclusion that was drawn from the results obtained was that a large performance benefit (C_L/C_D) was found for the Wortmann wing under propeller slipstream conditions (tractor configuration). The lift-to-drag ratio improvements were caused by the turbulated nature of the slipstream flow over the wing. The induced flow due to the propeller creates a region of fully turbulent flow on the central portion of the wing and induces the formation of the separation bubble over the rest of the wing at lower chordwise Reynolds numbers. The region of turbulent flow attenuates the pressure drag and increases the lift of the wing at angles of attack up to stall. In essence, the induced flow due to the propeller acts as a trip that most importantly works at low angles of attack.

Both the advance ratio and location variation experiments performed on the Wortmann wing have made it clear that the proper integration of the propeller-wing combination will result in large performance benefits at low Reynolds numbers. The benefits found from the experiments performed on the Wortmann wing can be translated to improved small-scaled UAV performance at most flight conditions (takeoff, cruise, and landing).

Acknowledgments

The authors thank Pritam P. Sukumar, Jeff Diebold, Or D. Dantsker, and Raylan Vaz for their assistance in wind tunnel testing. The authors would also like to thank Scott A. McDonald, Greggory L. Bennett, and David L. Switzer from the UIUC Electrical and Computer Engineering (ECE) machine shop for their guidance and support in machining the LRN-FB.

References

[1]Smelt, R. and Davies, H., "Estimation of Increase in Lift Due to Slipstream," ARC R&M 1788, 1937.

[2]Young, A. D. and Morris, D. E., "Note of Flight Tests on the Effect of Slipstream on Boundary Layer Flow," ARC R&M 1957, 1939.

[3]Young, A. D. and Morris, D. E., "Further Note of Flight Tests on the Effect of Slipstream on Boundary Layer Flow," RAE Rept. No. B.A. 1404b, 1939.

[4]Thompson, J. S., Smelt, R., Davison, B., and Smith, F., "Comparison of Pusher and Tractor Propeller Mounted on a Wing," ARC R&M 2516, 1940.

[5]Kuhn, R. E. and Draper, J. W., "Investigation of the Aerodynamic Characteristics of a Model Wing-Propeller Combination and of the Wing and Propeller Separately at Angles of Attack up to 90 deg," NACA 1263, 1956.

[6]Brenkmann, M., "Experimental Investigation of the Aerodynamics of a Wing in a Slipstream," UTIA 11, Toronto, ON, Canada, April 1957.

[7]Ribner, H. S., "Theory of Wings in Slipstreams," UTIA 60, Toronto, ON, Canada, May 1959.

[8]Loth, J. L. and Loth, F., "Induced Drag Reduction with Wing Tip Mounted Propellers," AIAA Paper 1984-2149, Seattle, WA, Aug. 1984.

[9]Patterson, J. C. and Barlett, G. R., "Effect of a Wing-Tip Mounted Pusher Turboprop on the Aerdynamic Characteristics of a Semi-span Wing," AIAA Paper 1985-1286, Monterey, CA, July 1985.

[10]Miranda, L. and Brennan, J., "Aerodynamic Effects of Wingtip-Mounted Propellers and Turbines," AIAA Paper 1986-1802, San Diego, CA, July 1986.

[11]Kroo, I., "Propeller-Wing Integration for Minimum Induced Loss," *Journal of Aircraft*, Vol. 23, No. 7, 1986, pp. 561–565.

[12]Munk, M., "Minimum Induced Drag of Airfoils," NACA Rept. 121, 1921.

[13]Veldhuis, L. L. M., "Review of Propeller-Wing Aerodynamic Interference," *24th International Congress of the Aeronautical Sciences*, Yokohama, Japan, 2004.

[14]Veldhius, L. L. M., *Propeller-Wing Aerodynamic Interference*, Ph.D. thesis, Dept. of Aerospace Engineering, Delft University of Technology, Delft, The Netherlands, June 2005.

[15]Witkowski, D. P., Johnston, R. T., and Sullivan, J. P., "Propeller/Wing Interaction," AIAA Paper 1989-0535, Reno, NV, 1989.

[16]Witkowski, D. P., Lee, A. K. H., and Sullivan, J. P., "Aerodynamic Interaction between Propellers and Wings," *Journal of Aircraft*, Vol. 26, No. 9, 1989, pp. 829–836.

[17]Catalano, F. M., "On the Effect of an Isolated Propeller Slipstream on Wing Aerodynamic Characteristics," *Acta Polytechnica*, Vol. 44, No. 3, 2004, pp. 8–14.

[18]Pines, D. J. and Bohorquez, F., "Challenges Facing Future Micro-Air-Vehicle Development," *Journal of Aircraft*, Vol. 43, No. 2, March–April 2006, pp. 290–305.

[19]Null, W., Noseck, A., and Shkarayev, S., "Effects of Propulsive-Induced Flow on the Aerodynamics of Micro Air Vehicles," AIAA Paper 2005-4616, Toronto, Ontario, June 2005.

[20]Shkarayev, S., Moschetta, J.-M., and Bataille, B., "Aerodynamic Design of Micro Air Vehicles for Vertical Flight," *Journal of Aircraft*, Vol. 45, No. 5, Sept.–Oct. 2008, pp. 1715–1724.

[21]Randall, R., Hoffmann, C.-A., and Shkarayev, S., "Longitudinal Aerodynamics of a Vertical Takeoff and Landing Micro Air Vehicle," *Journal of Aircraft*, Vol. 48, No. 1, Jan.–Feb. 2011, pp. 166–176.

[22]Randall, R., Wilson, L., and Shkarayev, S., "Flow Interactions around a Rapidly-Pitching MAV Wing," AIAA Paper 2012-0667, Nashville, TN, Jan. 2012.

[23]Sudhakar, S., Kumar, C., Arivoli, D., Dodamani, R., and Venkatakrishnan, L., "Experimental Studies of Propeller Induced Flow over a Typical Micro Air Vehicle," AIAA Paper 2013-0060, Grapevine, TX, Jan. 2013.

[24]Gamble, B. J. and Reeder, M. F., "Experimental Analysis of Propeller-Wing Interactions for a Micro Air Vehicle," *Journal of Aircraft*, Vol. 46, No. 1, 2009, pp. 65–73.

[25]Selig, M. S. and McGranahan, B. D., *Wind Tunnel Aerodynamic Tests of Six Airfoils for Use on Small Wind Turbines*, National Renewable Energy Laboratory, NREL/SR-500-35515, Golden, CO, 2004.

[26]Ananda, G. K., *Aerodynamic Performance of Low-to-Moderate Aspect Ratio Wings at Low Reynolds numbers*, Master's thesis, University of Illinois at Urbana-Champaign, Department of Aerospace Engineering, Urbana, IL, 2012.

[27]Ananda, G. K., Sukumar, P. P., and Selig, M. S., "Low-to-Moderate Aspect Ratio Wings Tested at Low Reynolds Numbers." AIAA Paper 2012-3026, New Orleans, LA, June 2012.

[28]Barlow, J. B., Rae, W. H., Jr., and Pope, A., *Low-Speed Wind Tunnel Testing, Third Ed.*, John Wiley and Sons, New York, 1999.

[29]Kline, S. and McClintock, F. A., "Describing Uncertainty in Single-Sample Experiments," *Mechanical Engineering*, Vol. 75, 1953, pp. 3–8.

[30]Coleman, H. W. and W. G. Steele, Jr., *Experimentation and Uncertainty Analysis For Engineers*, John Wiley and Sons, New York, 1989.

[31]Anonymous, "Realize,® Inc. Rapid Prototyping, Rapid Prototypes, Stereolithography," http://www.realizeinc.com/, Accessed Feb. 2012.

[32]Deters, R.W. and Selig, M.S., "Static Testing of Micro Propellers," AIAA Paper 2008-6246, Honolulu, HI, Jan. 2008.

[33]Brandt, J. B., *Small-Scale Propeller Performance at Low Speeds*, Master's thesis, University of Illinois at Urbana-Champaign, Department of Aerospace Engineering, Urbana, IL, 2005.